International Nano Letters (2018) 8:263–275
https://doi.org/10.1007/s40089-018-0249-z

ORIGINAL ARTICLE

Coexistence of filamentary and homogeneous resistive switching with memristive and meminductive memory effects in Al/MnO_2/SS thin film metal–insulator–metal device

Girish U. Kamble[1] · Nitin P. Shetake[1] · Suhas D. Yadav[1] · Aviraj M. Teli[2] · Dipali S. Patil[3] · Sachin A. Pawar[3] · Milind M. Karanjkar[4] · Pramod S. Patil[2] · Jae C. Shin[3] · Marius K. Orlowski[5] · Rajanish K. Kamat[6] · Tukaram D. Dongale[1]

Received: 16 July 2018 / Accepted: 10 September 2018 / Published online: 19 September 2018

Abstract

In the present investigation, we have experimentally demonstrated the coexistence of filamentary and homogeneous resistive switching mechanisms in single Al/MnO_2/SS thin film metal–insulator–metal device. The voltage-induced resistive switching leads to clockwise and counter-clockwise resistive switching effects. The present investigations confirm that the coexistence of both RS mechanisms is dependent on input voltage, charge-flux and time. Furthermore, the non-zero I–V crossing locations and crossovers hysteresis loops suggested that the developed device has memristive and meminductive properties. The memristive and meminductive memory effects are further confirmed by electrochemical impedance spectroscopy. The results suggested that the mem-device dynamics and electrochemical kinetics during different voltage sweeps and sweep rates are responsible for the coexistence of filamentary and homogeneous resistive switching mechanisms as well as memristive and meminductive memory effect in single Al/MnO_2/SS metal–insulator–metal device. The coexistence of both RS effects is useful for the development of high-performance resistive memory and electronic synapse devices. Furthermore, the coexistence of memristive and meminductive memory effects is important for the development of adaptive and self-resonating devices and circuits.

Keywords Memristor · Resistive switching (RS) · Filamentary RS · Homogeneous RS · Meminductive effect · MnO_2

Introduction

Resistive random access memory (RRAM) technology gained tremendous interest in the last few years as a future solution for the memory, logic, and computing applications [1–4]. One of the variants of the RRAM is a memristor or simply memory resistor [5, 6], which was theorized in 1971 [7] and experimentally demonstrated in 2008 [8]. The device structure of memristor is very similar to metal–insulator–metal (MIM) type and offers a lot of advantages in terms of footprint, speed, and power consumption [9]. In the recent years, different kinds of materials were used as an active layer; however, the oxide-based RRAM is popular due to the fast switching performance, higher endurance and retention, lower footprint, and CMOS compatibility [10]. In such devices, the resistive switching (RS) mechanism was governed by either homogeneous or filamentary type. In the case of homogeneous RS, the current is distributed homogeneously across the active layer, whereas formation and

Girish U. Kamble and Nitin P. Shetake contributed equally to this manuscript.

✉ Tukaram D. Dongale
tdd.snst@unishivaji.ac.in

[1] Computational Electronics and Nanoscience Research Laboratory, School of Nanoscience and Biotechnology, Shivaji University, Kolhapur 416004, India

[2] Department of Physics, Shivaji University, Kolhapur 416004, India

[3] Department of Physics, Yeungnam University, Gyeongsan, Gyeonbuk 38541, South Korea

[4] Department of Physics, Vivekanand College, Kolhapur 416003, India

[5] Bradley Department of Electrical and Computer Engineering, Virginia Tech., Blacksburg, VA 24061, USA

[6] Department of Electronics, Shivaji University, Kolhapur 416004, India

breaking of the conductive filament(s) responsible for the filamentary RS [11–14].

The homogeneous RS shows poor retention performance and suffers from contact resistance problem [6]. On the other hand, the filamentary RS suffers from scaling issues [1, 11]. The synergetic integration of homogeneous and filamentary RS may lead to highly scalable and efficient memory cells that would be useful for the CMOS-compatible RRAM and neuromorphic applications [15–19]. Considering the advantages of synergetic integration, many research groups come up with different solutions. Recently, Peng et al. [12] have demonstrated the coexistence of both RS mechanism by modifying the bottom electrodes. Similarly, Biju et al. [14] have shown the coexistence by modulating active layer thickness of MIM devices. However, the simultaneous coexistence of both RS mechanisms was missing in the above devices. The field-induced RS with the coexistence of filamentary and homogeneous RS in Fe-doped $SrTiO_3$ thin films [13], ZnO thin film memristor [20], $DyMn_2O_5$ memory devices [21] and $SrTiO_{3-\delta}$ RS bits [22] was reported recently. However, simultaneous homogeneous and filamentary RS mechanisms at same voltage or an electric field were absent in these devices. Furthermore, the coexistence of fundamental memelements (memristor, memcapacitor, and meminductor) memory properties was not reported for these devices. The memelements are the broader class of non-linear passive circuit elements and they are useful in the field of adaptive circuits and self-resonating devices.

In view of this, the present report demonstrates the voltage-induced coexistence of filamentary and homogeneous resistive switching with memristive and meminductive memory effects in MnO_2 thin film MIM device. The present report confirms that the coexistence of both RS mechanisms is dependent on input voltage, charge-flux and time.

Experimental

Materials and methods

The stainless steel (SS) substrate with 885 ± 3 μm thickness was used to deposit MnO_2 thin film. Potassium permanganate ($KMnO_4$) AR grade with purity 99% was purchased from SD Fine Pvt. Ltd., India and used as received. A double distilled water (DDW) was used to prepare all aqueous solutions. In this work, the MnO_2 thin film was deposited by a simple, cost-effective and environmentally benign hydrothermal method. In the beginning, the SS substrate was washed with laboratory detergent, then polished by zero-grade polish paper followed by washing with ethanol and concentrated HCl. In a typical experiment, the Mn precursor (3 mM $KMnO_4$) was dissolved in 50 mL DDW and stirred for 10 min. After the dissolution of Mn precursor, the ethanol–HCl-treated SS substrate was immersed in the solution by inclining it to the wall of the beaker. This beaker was kept in the automatic vertical autoclave (Bio-Technics, India) at 90 °C for 4 h and then allowed to cool to room temperature naturally. The SS substrate was removed from the autoclave and rinsed in DDW. This obtained thin film was dried at 60 °C for 3 h with the help of a hot air oven (Bio-Technics, India). Finally, the prepared thin film was used for further characterizations.

Device development

The MnO_2 thin film was deposited using a simple and cost-effective hydrothermal method. In order to create MIM structure, SS was used as a bottom electrode on which MnO_2 active layer was grown using the hydrothermal method. The top Aluminum (Al) layer was developed using thermal evaporation technique (Vacuum Techniques, Bengaluru, Model—VT-ACG-03). In the typical process, Al evaporation slugs with 99.99% purity were purchased from Sigma-Aldrich and placed in the Molybdenum evaporation boat. The MnO_2/SS system was placed in the vacuum chamber and 10^{-5} Torr vacuum environment was created to develop good quality Al electrode. The Al metal was evaporated by passing 85 A current through the evaporation boat which contains Al evaporation slugs. The uniformity of the top electrode was assured by maintaining the optimized distance (23 cm) between boat and substrate holder and contamination-free Al evaporation slugs.

Characterizations of MnO_2 thin film MIM device

Raman spectra of MnO_2 thin film was recorded using a Raman spectrometer (Bruker MultiRAM, Germany). The surface morphology of MnO_2 thin film was examined using Field Emission Scanning Electron Microscope (FESEM) (S-4700, Hitachi). The electrical characterization of Al/MnO_2/SS MIM device was recorded using programmable electrochemical workstation (Autolab N-Series). In the present investigation, the top Al electrode was biased, while bottom SS electrode was grounded during all measurements. The current–voltage (I–V) characteristic of the Al/MnO_2/SS MIM device was recorded by applying the sweep voltage in the order of ± 1 V, ± 1.5 V, ± 2 V, ± 3 V, ± 4 V and ± 5 V across the device with sweep rate increased from 100 to 500 mV/s. The electrochemical impedance spectroscopy (EIS) studies were carried out using 10 mV_{AC} amplitude with frequencies sweeping from 10 Hz to 1 MHz. Surface profiler (AMBiOS XP-1) was used to determine the thickness of the active layer and the top electrode. The thickness of the MnO_2 active layer and top Al electrode was found to be 13 ± 2 μm and 350 ± 10 nm, respectively.

Results and discussion

Figure 1 shows typical Raman spectra of the hydrothermally synthesized MnO_2 thin film at 3 mM concentration of Mn precursor, for 4-h deposition time. The vibration absorption peaks of Mn–O–Mn bonds are located at 573 cm^{-1} and 647 cm^{-1} in the spectral region 300–800 cm^{-1} corresponds to MnO_2. These absorption peaks in the spectral region are due to stretching vibrations of MnO_6 octahedral and in good agreement with the formation of birnessite-type MnO_2, confirmed by previously reported literature [23–25]. The nanostructures of MnO_2 prepared by hydrothermal method were examined using FESEM, as shown in Fig. 2a, b. At the lower magnification (50 k), the wood dust-like nanostructure is clearly observed. The semi-compact nature of MnO_2 thin film with nanostructures of ~ 300 nm is clearly observed at higher magnification (100 k) as shown in Fig. 2b.

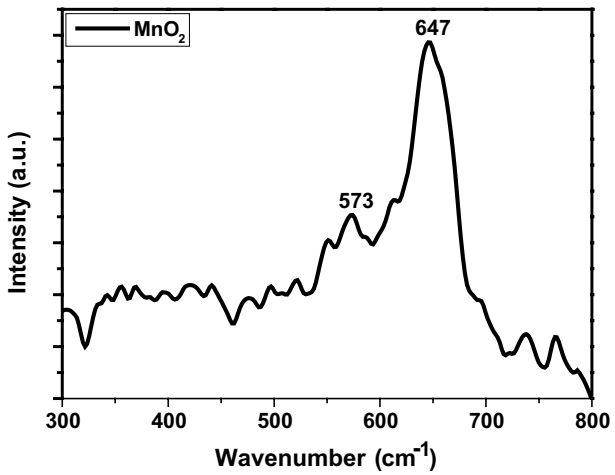

Fig. 1 Raman scattering spectra of hydrothermally synthesized MnO_2 thin film at 3 mM concentration of Mn precursor, for 4-h deposition time

According to resistive switching polarity, resistive memories are classified into two types viz. unipolar and bipolar. Furthermore, filamentary and homogeneous RS mechanisms are commonly explored in resistive memory devices [26]. The RS effect is dependent on various parameters such as device structure, active material, top and bottom electrodes, external voltage stimulus, doping, the interface between the active layer and electrodes, etc. [27–29]. In the present investigation, we have investigated the voltage-induced RS effect in the Al/MnO_2/SS thin film MIM device and demonstrated the coexistence of filamentary and homogeneous RS with memristive, meminductive and nanobattery effects. Figure 3 represents the exemplary I–V characteristics of Al/MnO_2/SS MIM device. I–V characteristic was measured at 1.5 V with sweep rate equals to 500 mV/s. Typical hysteresis loop in I–V plane is clearly observed for the developed device, which is fingerprint characteristic of the memristive device [30–32]. The memristive hysteresis loops are observed in many material systems such as oxides, ferrites, polymers, biomaterials, etc. and it is very similar to the resistive switching effect. In the case of memristive/resistive switching, device undergoes the change in the resistance state with the application of a certain bias (SET or RESET voltages). In the case of filamentary RS, the well-grown conductive filament is formed at the SET voltage and breaks at the RESET voltage. The direction of switching decides the RS mode (homogeneous and filamentary) and dictates device performance. For this case, I–V hysteresis loop was followed in the sequence $0 \rightarrow +V_{max} \rightarrow 0 \rightarrow -V_{max} \rightarrow 0$ which represents the clockwise switching (CWS). The clockwise transition from ON state to OFF was indicated by arrows. It is interesting to note that the two different types of switching with opposite directions are observed with the application of different voltage sweeps (± 1 to ± 5 V). The upper inset shows the

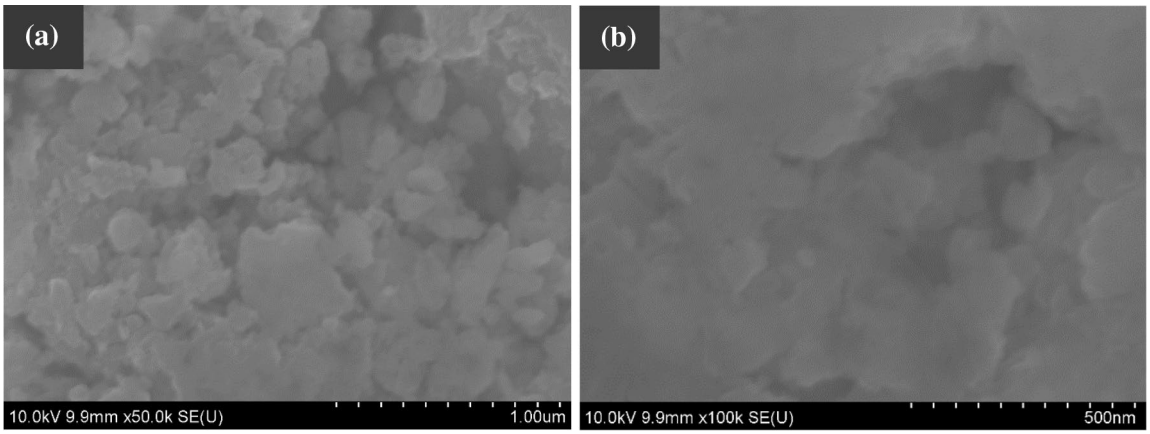

Fig. 2 FESEM images of hydrothermally synthesized MnO_2 thin film at **a** lower magnification (50 k) and **b** higher magnification (100 k)

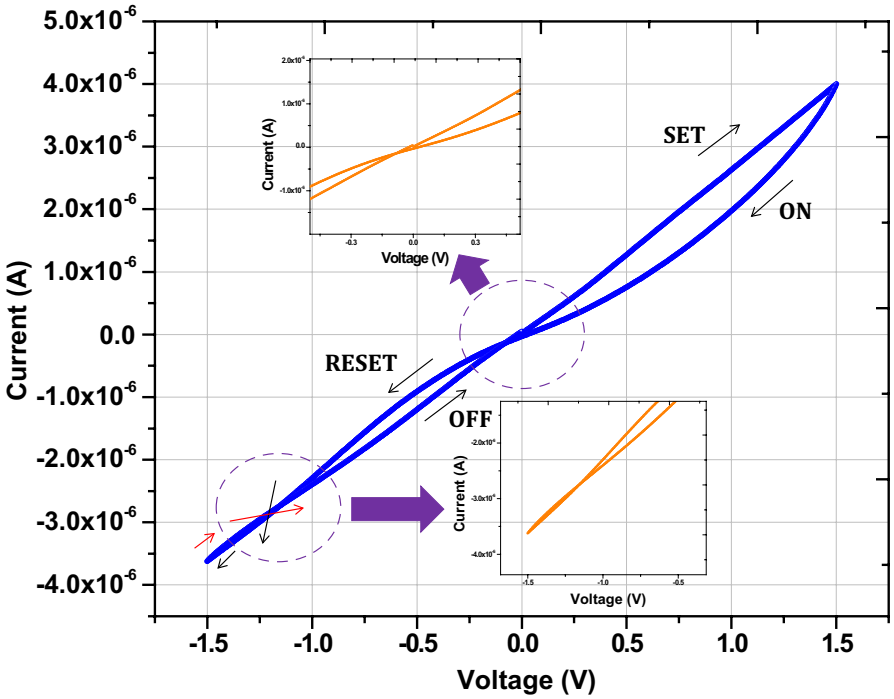

Fig. 3 Typical current–voltage (I–V) hysteresis loop of Al/MnO_2/SS MIM device measured at sweep rate equal to 500 mV/s with ± 1.5 V sweep voltage. The upper inset shows the zoomed view of the non-zero-crossing property and the lower inset shows the zoomed view of crossover hysteresis

zoomed view of non-zero I–V crossing property and the lower inset shows the zoomed view of crossover hysteresis. Recently, Qingjiang et al. have demonstrated that the non-zero I–V crossing property or shifting of I–V crossing in the first or third quadrant results in a coexistence of memcapacitive and meminductive properties with memristive effect, respectively [32]. In other words, one can use this simple test to identify the coexistence of memory effects and differentiate the non-ideal memristive devices from ideal memristor or generic memristor devices. In the present report, we have demonstrated the voltage-induced coexistence of filamentary and homogeneous resistive switching with memristive and meminductive memory properties in the MnO_2 thin film. The coexistence of memristive and meminductive memory effects is further analyzed by EIS.

The detailed voltage-induced RS effect of the Al/MnO_2/SS thin film MIM device is shown in Fig. 4a–f. To get two different types of switching with opposite direction, we have varied the sweep voltages as ± 1 V, ± 1.5 V, and ± 2 V to ± 5 V. After careful analysis of I–V loops and branching directions during all voltage sweeps and sweep rates, three different modes of operation were observed. In the first mode, the counter-clockwise switching (CCWS) was observed for ± 1 V voltage sweep in which I–V hysteresis followed the sequence $0 \rightarrow +V_{max} \rightarrow 0 \rightarrow -V_{max} \rightarrow 0$, as shown in Fig. 4a. In the second case, with a further increase in sweeping voltage to 1.5 V, the switching direction was reversed. The switching was in the sequence $0 \rightarrow +V_{max} \rightarrow 0 \rightarrow -V_{max} \rightarrow 0$ which represents the clockwise switching (CWS), as shown in Fig. 4b. The third mode of operation was the accumulation of the previous two modes. The branching direction and I–V loops of ± 2 V to ± 5 V sweeping voltages were shown in Fig. 4c–f. In this case, the upper loops follow the CWS, whereas the lower loops follow the CCWS. It was observed that irrespective of any voltage sweep, the sequence of RS was found to be same i.e., $0 \rightarrow +V_{max} \rightarrow 0 \rightarrow -V_{max} \rightarrow 0$. By careful observations of I–V loops during the measurements, change was observed only in the branching direction and not in the sweeping voltage polarity. Recently, Münstermann et al. [13] and Biju et al. [14] have reported that the CCWS represents the homogeneous RS whereas CWS represents the filamentary RS. In the present case, the first mode represents the homogeneous RS, the second mode represents the filamentary RS, and the third mode represents the simultaneous filamentary and homogeneous RS. The field-induced change of the Schottky barrier at the interface of the electrode and the active material is the agreed reason for the homogeneous RS; whereas, the formation and breaking of the conductive filaments are responsible for the filamentary RS [13, 14, 29].

In mode- 1, the slower switching kinetics at ± 1 V creates an asymmetric balance of Schottky-barrier heights which results in the homogeneous RS. In mode 2, the switching kinetics gets improved for higher voltage (± 1.5 V) which facilitates the redistribution of charge carriers to form a conductive filament which results in the filamentary RS. Further increase in the voltage (± 2 to ± 5 V; mode 3), the positive bias creates the conductive filament, whereas oxygen vacancies were detached from the conductive filament during the negative bias. It was possible for detached

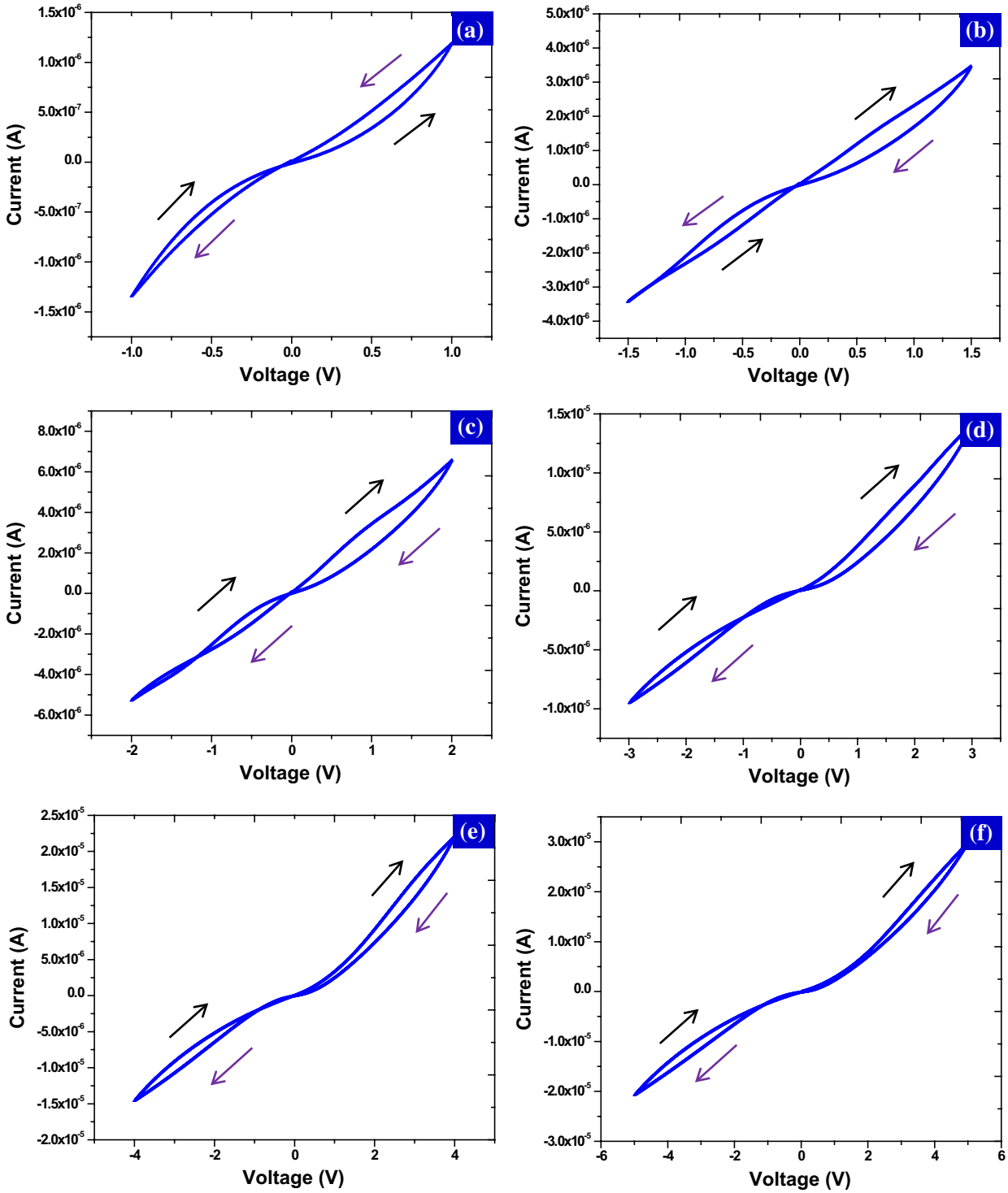

Fig. 4 Bipolar resistive switching characteristics of Al/MnO_2/SS MIM device measured at sweep rate equal to 300 mV/s with sweep voltages **a** ±1 V; **b** ±1.5 V; **c** ±2 V; **d** ±3 V; **e** ±4 V; **f** ±5 V, respectively. The arrow indicates the direction of resistive switching

oxygen vacancies to concentrate near the top electrode. These detached oxygen vacancies may create many percolation channels near the top Al electrode which impedes to form a complete conductive filament. This process results in the homogeneous RS. These percolation channels are also responsible for the meminductive effect [32]. In the nutshell, the different charge carrier densities beneath the top Al electrode with the application of different external bias

are responsible for the coexistence of filamentary and homogeneous resistive switching effect. Considering the above facts, the modulation of sweeping voltage leads to the tuning of RS either filamentary, homogeneous or both at the same time. The sweep rate (charge-flux and time)-dependent maximum positive (I_{SET}) and negative current (I_{RESET}) is shown in Fig. 5a, b. Furthermore, the typical analog memory of Al/MnO_2/SS MIM device measured at ± 1.5 V and ± 5.0 V with sweep rate equal to 100–500 mV/s is shown in Fig. 5c, d. The results clearly indicate that the current tends to increase as both switching mechanisms dominate at higher sweep voltages and sweep rates. From our experiments and by comparing the previous reports [13, 14, 22], we can conclude that the coexistence of both the RS mechanisms is dependent on an input voltage or electric field, similar to [13, 22] and charge-flux and time [22].

The coexistence of both the RS is useful for the neuromorphic applications. In such applications, analog switching with an increase in the synaptic weights can mimic through the homogeneous RS, whereas the better resistance retention properties can be achieved through filamentary RS [11]. To check the suitability of Al/MnO_2/SS thin film MIM device for neuromorphic application, we have plotted the maximum positive (I_{SET}) and negative current (I_{RESET}) with different sweep rates at different resistive switching voltages and analog memory as shown in Fig. 5a–d, respectively. It is observed that the current increases in both the bias regions with an increase in voltage sweeps and sweep rates. In the biological synapse, improvement in the strength of synaptic weights results in the better learning [33]. In many memristive-based electronic synapses, current (i) was considered as synaptic weights [33–35]. Considering the incremental I_{SET} and I_{RESET} or synaptic weights, the Al/MnO_2/SS MIM device is suitable for the neuromorphic applications.

The pinched hysteresis loop in I–V plane with exact crossing at origin results in an ideal memristor [36–38].

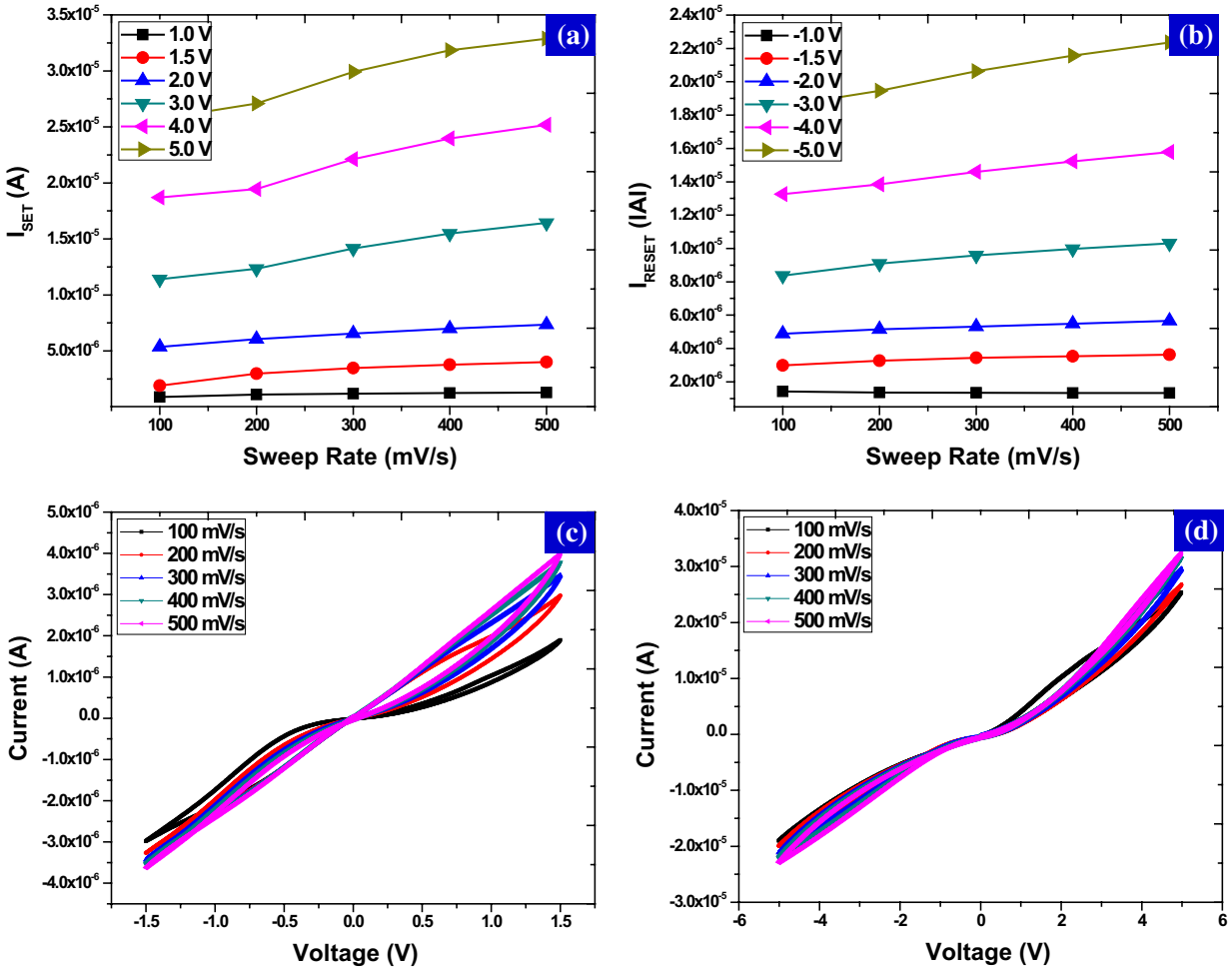

Fig. 5 Maximum positive and negative current (I_{SET} and I_{RESET}) with different sweep rates at different voltage sweeps for **a** positive bias region and **b** negative bias region. The typical analog memory of Al/MnO_2/SS MIM device measured at **c** ± 1.5 V and **d** ± 5.0 V with sweep rate equal to 100–500 mV/s

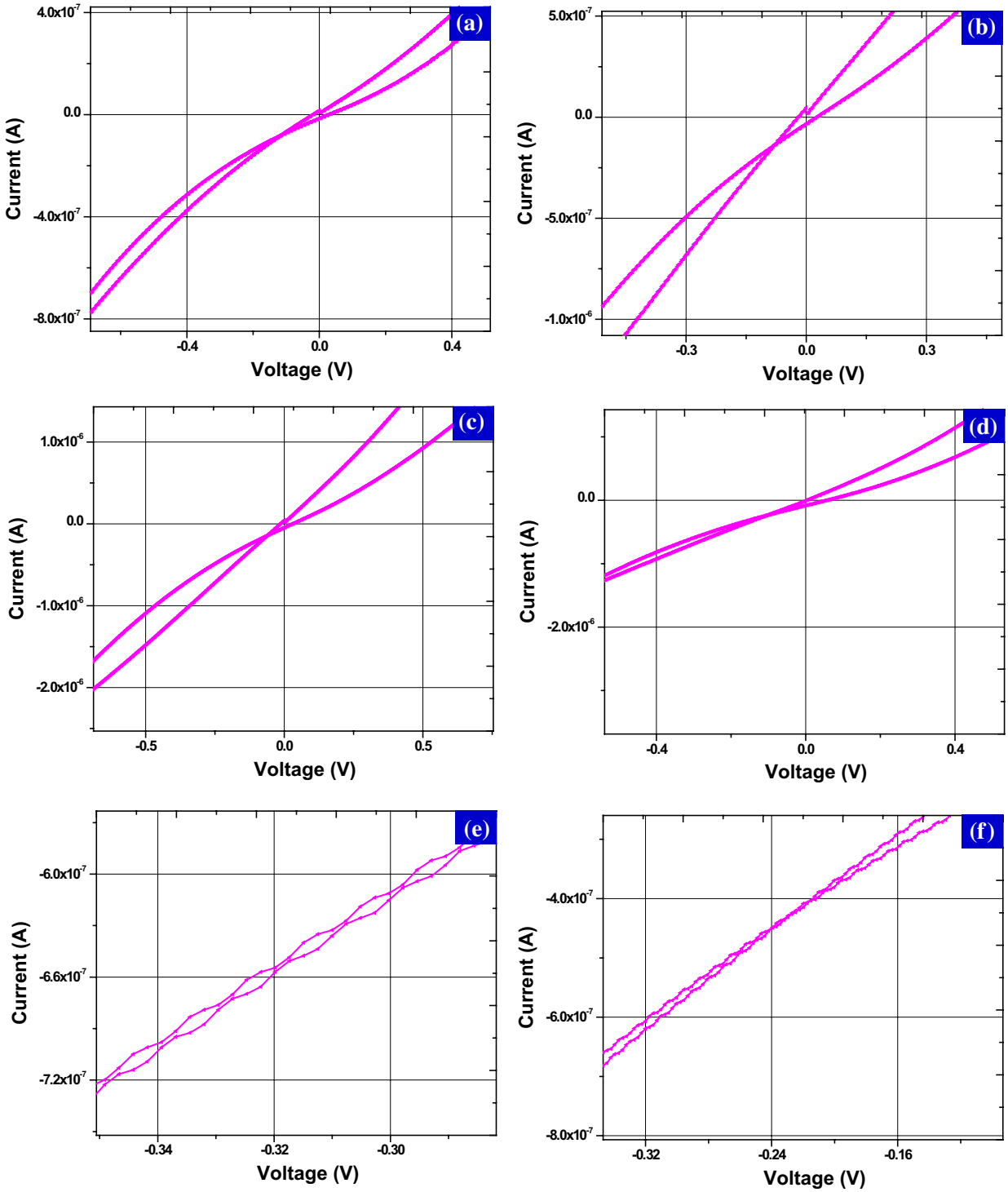

Fig. 6 The non-zero I–V crossing location at negative bias for sweep voltages **a** ±1 V; **b** ±1.5 V; **c** ±2 V; **d** ±3 V; **e** ±4 V; **f** ±5 V, respectively. All plots correspond to 500 mV/s sweep rate

Recently, memcapacitive and meminductive circuit elements were theorized and experimentally demonstrated [39, 40]. These are the broader class of non-linear passive circuit elements, which incorporates non-ideal behavior of memristor. However, most of the literature focused on the development of memristor or memristive devices by emphasizing zero crossing property. Recently, Valov et al. [31], Saraf et al. [41], and Tappertzhofen et al. [42] have reported

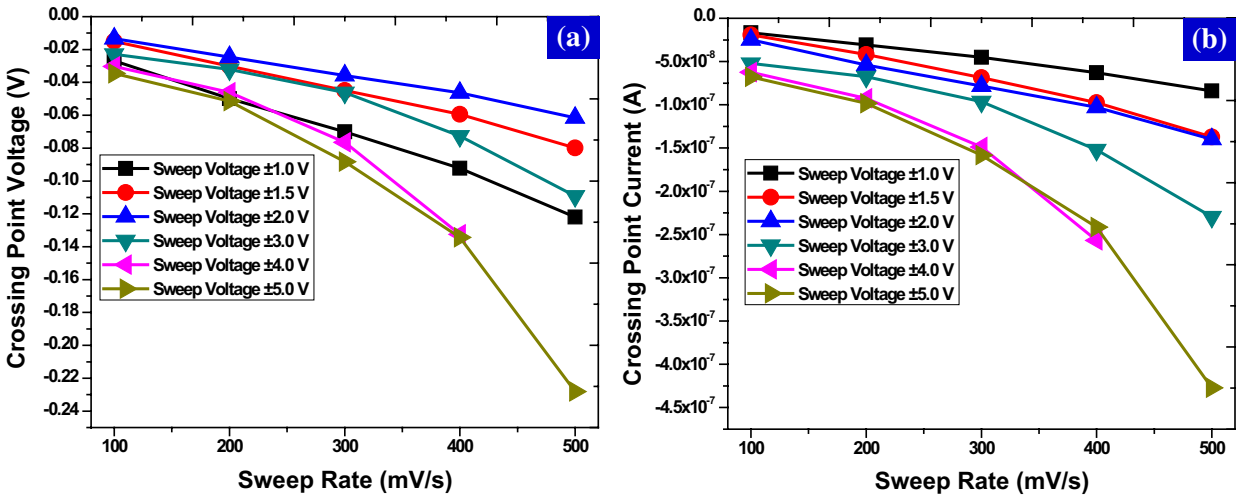

Fig. 7 The non-zero I–V crossing point locations of Al/MnO_2/SS MIM device at negative bias region; **a** crossing point voltages and corresponding **b** current locations with different sweep voltages and sweep rates

the non-zero crossing property of different MIM devices. Furthermore, the coexistence of memristance and meminductance memory effects in the single device was experimentally demonstrated by the Qingjiang et al. and proved that the shifting of I–V crossing location to the third quadrant leads to simultaneous memristive and meminductive memory effects in a single device [32].

In the present investigation, we have observed the additional meminductive effect along with the memristive property. Furthermore, we have observed that the non-zero I–V crossing location or meminductive effect is dependent on the voltage sweeps and sweep rates as against different frequencies methodology used in Ref. [32]. Figures 6a–f and 7a, b represent the non-zero I–V crossing property of developed MIM device, which was measured at 500 mV/s sweep rate with different sweep voltages. The results clearly indicate that the non-zero crossing point voltages and the corresponding magnitude of current increase as the sweep rate and sweep voltage increase. These results are consistent with the results reported in the Ref. [41]. It is interesting to know that the 'memristor type-II'-like characteristic was observed for the ± 4 V sweep voltage (sweep rate − 500 mV/s). If the memory element shows self-crossing I–V loop at the origin, then it is called as a type-I memristor. On the other hand, if the memory element shows tangential I–V loop at the origin, then it is called as a type-II memristor [40, 41]. The detailed explanation of the hysteresis loop and its characteristics can be found in the Ref. [40, 41]. In the present case, the I–V loop does not cross each other and only shows the 'touch-and-go' behavior [43]. However, 'memristor type-II'-like characteristic was not observed for other sweep voltages and sweep rates. This kind of behavior may be due to the stochastic nature of RS mechanism [35, 44]. Figure 8a–f represents the crossover hysteresis loops of the developed MIM device. For most of the cases, only one crossover hysteresis loop was observed. Furthermore, three crossover hysteresis loops were present for the ± 3 V sweep voltage and no crossover hysteresis loops were observed for the ± 1 and ± 4 V sweep voltages. The detailed crossover hysteresis voltages and current locations are shown in the Fig. 9a, b. The results suggested that the crossover hysteresis voltages and current locations tend to decrease as the sweep rate and sweep voltages increase.

To calculate the resistive, capacitive, and inductive contributions to the mem-device dynamics and understand electrochemical kinetics, we have characterized the Al/MnO_2/SS MIM device using EIS and calculated the impedance parameters by fitting equivalent circuit model. The details of the impendence parameters are summarized in Table 1. The Nyquist plots of MIM device for different sweep voltages are shown in Fig. 10a–f and its equivalent circuit model is shown in the inset of Fig. 10a. The semicircles of Al/MnO_2/SS MIM device suggest the active cell could be modeled as a series resistor and an inductor with the parallel combination of a resistor and a capacitor. Two different impedance spectra for the ON and OFF states were observed for each sweep voltage. The area under the curve for OFF state was found to be higher than the ON state, which confirmed that the OFF state represents the high resistance state, whereas ON state represents the low resistance state. The series resistance (R_S) represents the lead resistance or contact resistance between measuring probe and top electrode whereas parallel resistance (R_P) represents the switching resistance [22, 45]. The inductive values during OFF state were found to be higher than the ON state for all sweep voltages. The inductive nature may have occurred due to the fact that the direction of net current is opposite to applied electric field

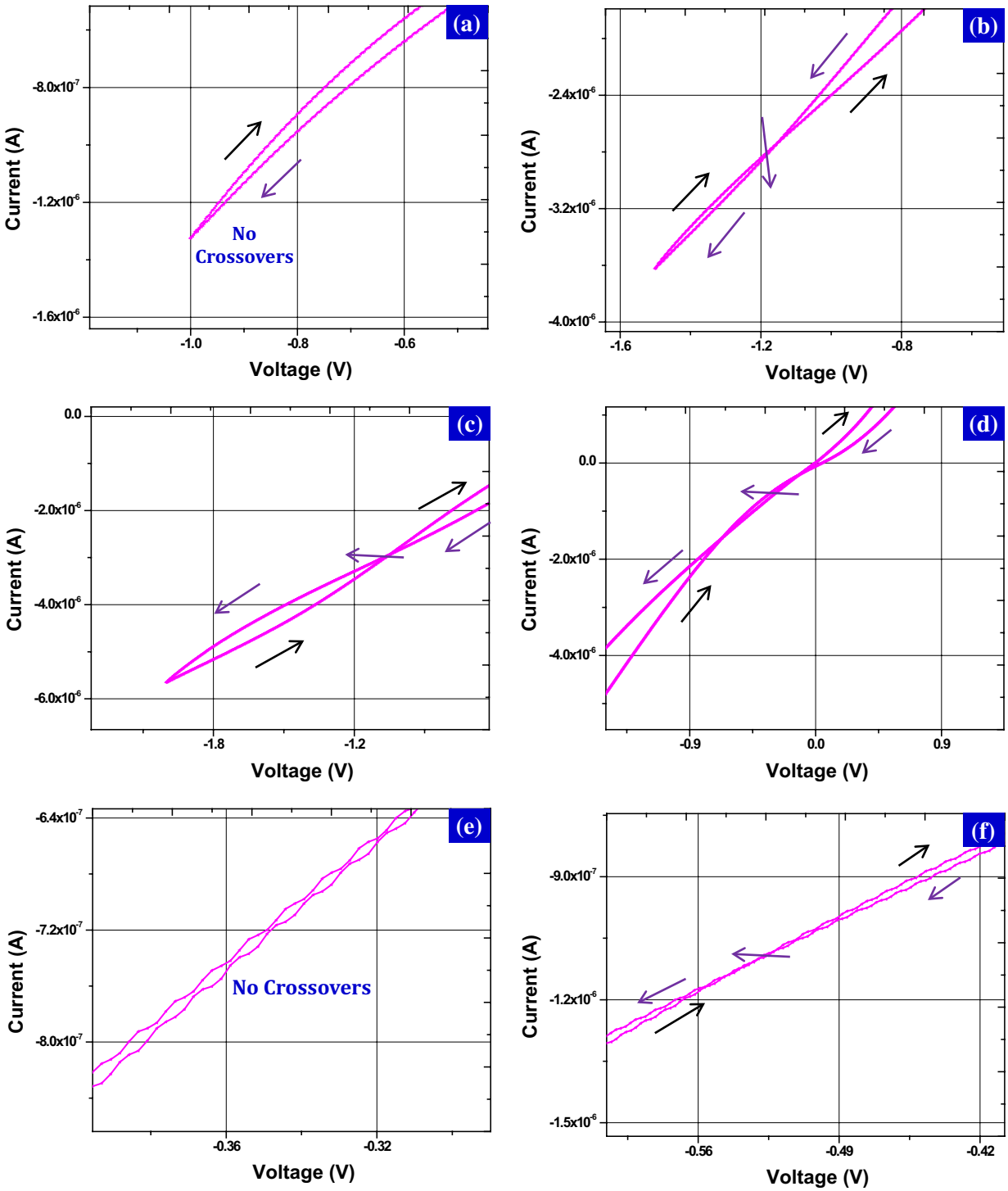

Fig. 8 The crossover hysteresis loops at sweep voltages **a** ±1 V; **b** ±1.5 V; **c** ±2 V; **d** ±3 V; **e** ±4 V; **f** ±5 V, respectively. The arrow indicates the direction of resistive switching. All plots correspond to 500 mV/s sweep rate

and diffusion relaxation [46]. These results further confirm that the meminductive behavior was prominent during OFF state and support the results reported in Ref. [32]. The percolation channels formed during OFF state were facilitated to form the winding conductive filaments which result in the significant meminductance effect in the MIM device [32]. These results reported herein suggest that the meminductive behavior can be found out by checking (1) shifting of I–V

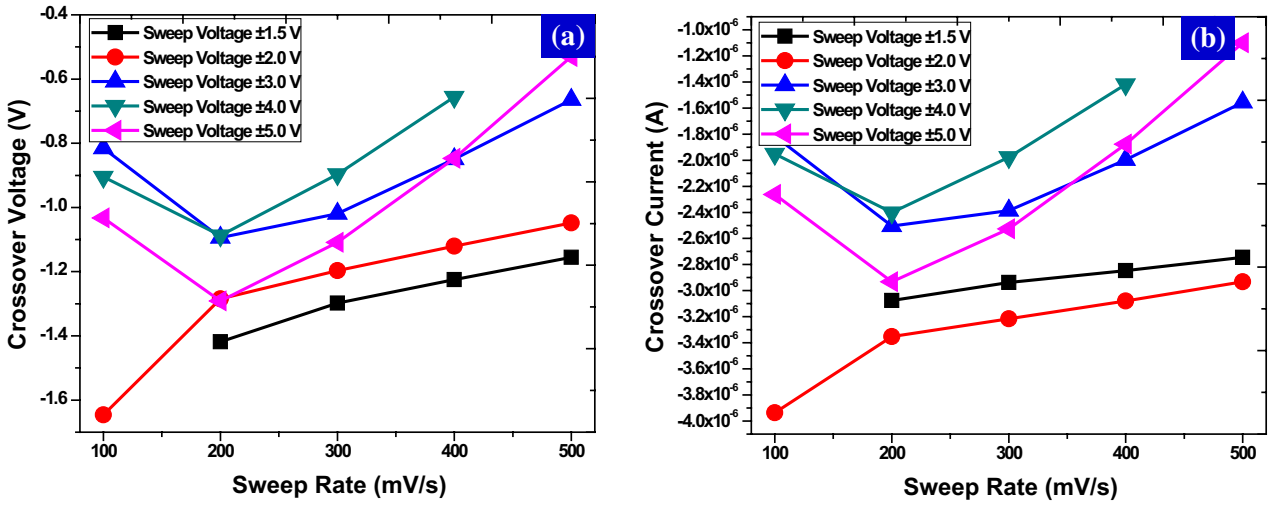

Fig. 9 The crossover hysteresis loops' locations of Al/MnO_2/SS MIM device at negative bias region; **a** crossover voltages and corresponding **b** current locations with different sweep voltages and sweep rates. No crossover hysteresis loops were observed for ± 1 and ± 4 V sweep voltage

crossing location to the third quadrant and (2) higher OFF state inductive behavior than ON state from EIS spectra. The coexistence of both RS effects will be useful for the development of high-performance resistive memory devices and electronic synapses. Furthermore, the coexistence of memristive and meminductive memory effects will be important for the development of adaptive circuits and self-resonating devices.

Conclusion

In conclusion, we have demonstrated the coexistence of filamentary and homogeneous RS mechanisms in single Al/MnO_2/SS MIM device using a voltage-induced RS effect.

Table 1 Impedance parameters of Al/MnO_2/SS MIM device (positive bias: ON state and negative bias: OFF state)

Sweep voltage (V)	R_S (Ω)	R_P (Ω)	L (mH)	CPE
1.0	2.96×10^4	2.00×10^5	3.093	8.21×10^{-10}
−1.0	3.01×10^4	2.60×10^5	3.598	6.65×10^{-10}
1.5	2.80×10^4	1.49×10^5	2.962	9.22×10^{-10}
−1.5	3.90×10^4	3.10×10^5	6.591	5.83×10^{-10}
2.0	2.51×10^4	1.42×10^5	2.473	2.57×10^{-09}
−2.0	3.96×10^4	2.74×10^5	6.270	4.66×10^{-10}
3.0	2.34×10^4	1.30×10^5	2.580	5.15×10^{-09}
−3.0	3.83×10^4	2.16×10^5	6.119	3.57×10^{-10}
4.0	2.31×10^4	1.35×10^5	2.817	4.26×10^{-09}
−4.0	3.62×10^4	2.09×10^5	5.170	3.08×10^{-10}
5.0	2.55×10^4	0.98×10^5	3.074	2.72×10^{-09}
−5.0	3.15×10^4	1.33×10^5	3.904	4.48×10^{-10}

Three modes of operation were observed during sweep voltage and sweep rate variations. The first mode represents CCWS (homogeneous RS), the second mode represents CWS (filamentary RS), and simultaneous CCWS and CWS were observed in the third mode. The third mode represents the coexistence of filamentary and homogeneous RS mechanisms in a single device. The accumulation of charge carrier densities beneath the top Al electrode with the application of different voltages is responsible for the coexistence of filamentary and homogeneous RS effect. The present report confirms that the coexistence of both the RS mechanisms is dependent on input voltage, charge-flux and time. The non-zero I–V crossing locations and crossover hysteresis loops suggested that the developed device has memristive and meminductive properties. The results suggested that the non-zero I–V crossing locations and corresponding current increases as the sweep rate and sweep voltage increases. Furthermore, the crossover hysteresis voltage and current locations tend to decreases as the sweep rate and sweep voltages increases. The memristive and meminductive memory effect is further confirmed by EIS. The results of equivalent circuit fitting suggest that the active cell could be modeled as a series resistor and an inductor with the parallel combination of a resistor and a capacitor. The resistance during OFF state was found to be higher than ON state of the device for each sweep voltage. Similarly, the inductive values during OFF state were found to be higher than the ON state values. These results further confirm that the meminductive behavior was dominant during OFF state due to the percolation channels and winding conductive filaments. The results suggested that the mem-device dynamics and electrochemical kinetics play an important role in the RS and memelements memory effects. The coexistence of homogeneous and filamentary

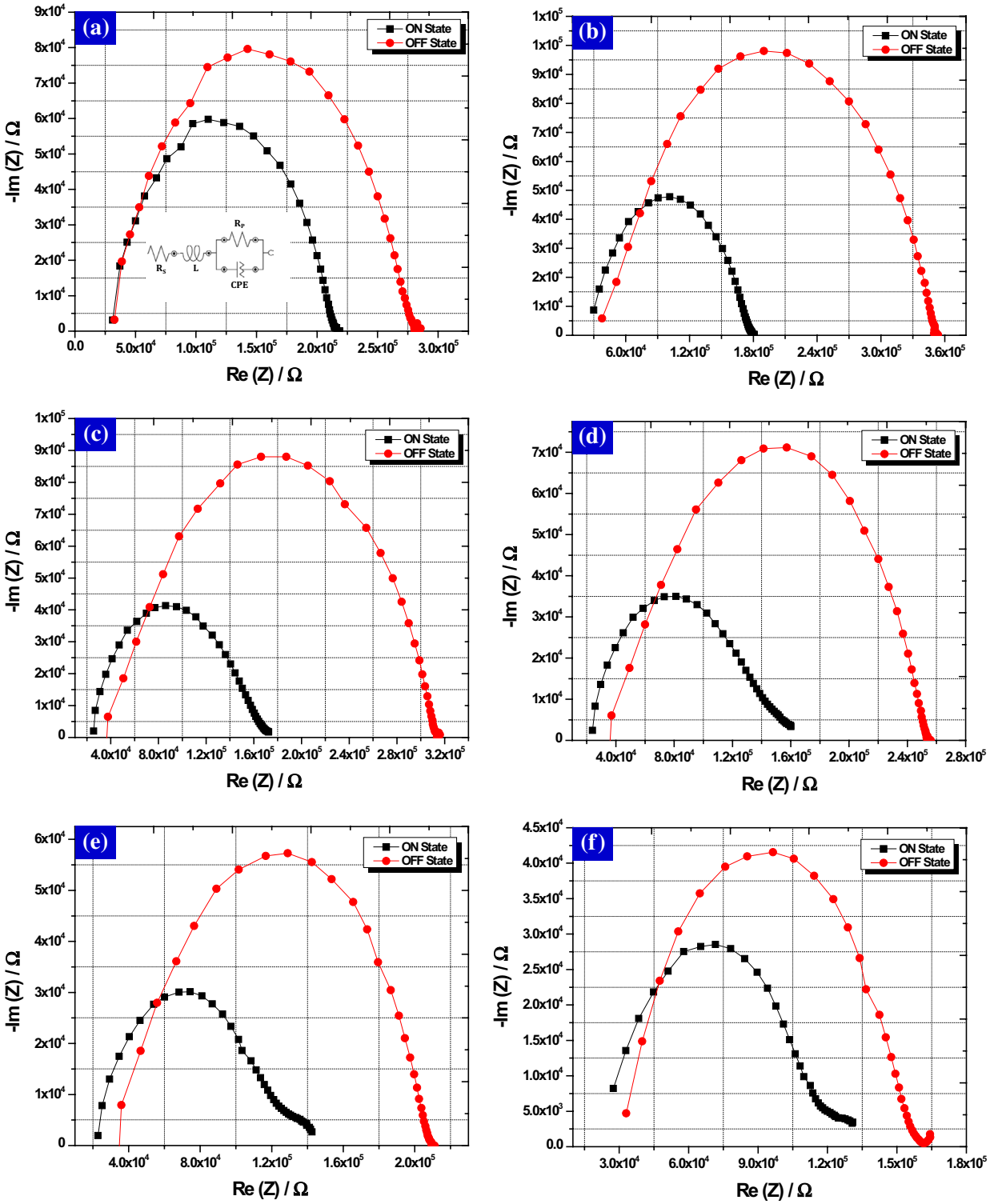

Fig. 10 Nyquist plots of Al/MnO_2/SS MIM device for sweep voltages **a** ±1 V; **b** ±1.5 V; **c** ±2 V; **d** ±3 V; **e** ±4 V; **f** ±5 V, respectively. The equivalent circuit of the device is shown in the inset of (**a**)

RS effects could be used to develop scalable and efficient memory cells for resistive memory and neuromorphic applications. Furthermore, adaptive and self-resonating devices and circuits could be easily developed by properly engineering the memristive and meminductive memory effects in the single device.

Acknowledgements The authors thank the Staff and Students of Physics Instrumentation Facility Centre (PIFC), Shivaji University, Kolhapur for valuable discussion and characterizations.

References

1. Meena, J., Sze, S., Chand, U., Tseng, T.Y.: Overview of emerging nonvolatile memory technologies. Nanoscale Res. Lett. **9**, 526 (2014)
2. Tarkhan, M., Nejad, M.M.: Design of a memristor based fuzzy processor. AEU Int. J. Electron. Commun. **84**, 331 (2018)
3. Anusudha, T.A., Prabaharan, S.R.S.: A versatile window function for linear ion drift memristor model—a new approach. AEU Int. J. Electron. Commun. **90**, 130 (2018)
4. Babacan, Y., Yesil, A., Kacar, F.: Memristor emulator with tunable characteristic and its experimental results. AEU Int. J. Electron. Commun. **81**, 99 (2017)
5. Babacan, Y., Kaçar, F.: Memristor emulator with spike-timing-dependent-plasticity. AEU Int. J. Electron. Commun. **73**, 16 (2017)
6. Yesil, A.: A new grounded memristor emulator based on MOSFET-C. AEU Int. J. Electron. Commun. **91**, 143 (2018)
7. Chua, L.: Memristor-the missing circuit element. IEEE Trans. Circuit Theory **18**, 507 (1971)
8. Strukov, D.B., Snider, G.S., Stewart, D.R., Williams, R.S.: The missing memristor found. Nature **453**, 80 (2008)
9. Kim, K.H., Gaba, S., Wheeler, D., Cruz-Albrecht, J.M., Hussain, T., Srinivasa, N., Lu, W.: A functional hybrid memristor crossbar-array/CMOS system for data storage and neuromorphic applications. Nano Lett. **12**, 389 (2012)
10. Sassine, G., Barbera, S.L., Najjari, N., Minvielle, M., Dubourdieu, C., Alibart, F.: Interfacial versus filamentary resistive switching in TiO_2 and HfO_2 devices. J. Vac. Sci. Technol. **B34**, 012202 (2016)
11. Simanjuntak, F.M., Panda, D., Wei, K.H., Tseng, T.Y.: Status and prospects of ZnO-based resistive switching memory devices. Nanoscale Res. Lett. **11**, 368 (2016)
12. Peng, H., Li, G., Ye, J., Wei, Z., Zhang, Z., Wang, D., Xing, G., Wu, T.: Electrode dependence of resistive switching in Mn-doped ZnO: filamentary versus interfacial mechanisms. Appl. Phys. Lett. **96**, 192113 (2010)
13. Muenstermann, R., Menke, T., Dittmann, R., Waser, R.: Coexistence of filamentary and homogeneous resistive switching in Fe-doped $SrTiO_3$ thin-film memristive devices. Adv. Mater. **22**, 4819 (2010)
14. Biju, K.P., Liu, X., Kim, S., Jung, S., Park, J., Hwang, H.: Coexistence of filamentary and homogeneous resistive switching in graded WO_x thin films. Phys. Status Solidi RRL **5**, 89 (2011)
15. Khot, A.C., Desai, N.D., Khot, K.V., Salunkhe, M.M., Chougule, M.A., Bhave, T.M., Kamat, R.K., Musselman, K.P., Dongale, T.D.: Bipolar resistive switching and memristive properties of hydrothermally synthesized TiO_2 nanorod array: effect of growth temperature. Mater. Des. **151**, 37 (2018)
16. Dongale, T.D., Desai, N.D., Khot, K.V., Volos, C.K., Bhosale, P.N., Kamat, R.K.: An electronic synapse device based on TiO_2 thin film memristor. J. Nanoelectron. Optoelectron. **13**, 68 (2018)
17. Mullani, N.B., Patil, V.B., Tikke, R.S., Pawar, P.S., Mohite, S.V., Bagade, A.A., Dongale, T.D.: Effect of Ag-doping on the hydrothermally grown ZnO thin film electronic synapse device. Bioinspired Biomim. Nanobiomater. **7**, 82 (2018)
18. Dongale, T.D., Mohite, S.V., Bagade, A.A., Kamat, R.K., Rajpure, K.Y.: Bio-mimicking the synaptic weights, analog memory, and forgetting effect using spray deposited WO_3 memristor device. Microelectron. Eng. **183**, 12 (2017)
19. Pawar, P.S., Tikke, R.S., Patil, V.B., Mullani, N.B., Waifalkar, P.P., Khot, K.V., Teli, A.M., Sheikh, A.D., Dongale, T.D.: A low-cost copper oxide thin film memristive device based on successive ionic layer adsorption and reaction method. Mater. Sci. Semicond. Process. **71**, 102 (2017)
20. Huang, C.H., Huang, J.S., Lai, C.C., Huang, H.W., Lin, S.J., Chueh, Y.L.: Manipulated transformation of filamentary and homogeneous resistive switching on ZnO thin film memristor with controllable multistate. ACS Appl. Mater. Interfaces **5**, 6017 (2013)
21. Tsai, Y.T., Chang, T.C., Huang, W.L., Huang, C.W., Syu, Y.E., Chen, S.C., Sze, S.M., Tsai, M.J., Tseng, T.Y.: Investigation for coexistence of dual resistive switching characteristics in $DyMn_2O_5$ memory devices. Appl. Phys. Lett. **99**, 092106 (2011)
22. Kubicek, M., Schmitt, R., Messerschmitt, F., Rupp, J.L.M.: Uncovering two competing switching mechanisms for epitaxial and ultrathin strontium titanate-based resistive switching bits. ACS Nano **9**, 10737 (2015)
23. Kim, M., Hwang, Y., Kim, J.: Graphene/MnO_2-based composites reduced via different chemical agents for supercapacitors. J Power Sources **239**, 225 (2013)
24. Ede, S.R., Anantharaj, S., Nithiyanantham, U., Kundu, S.: DNA-encapsulated chain and wire-like β-MnO_2 organosol for oxidative polymerization of pyrrole to polypyrrole. Phys. Chem. Chem. Phys. **17**, 5474 (2015)
25. Xie, Y., Yu, Y., Gong, X., Guo, Y., Guo, Y., Wang, Y., Lu, G.: Effect of the crystal plane figure on the catalytic performance of MnO_2 for the total oxidation of propane. CrystEngComm **17**, 3005 (2015)
26. Jeong, D.S., Thomas, R., Katiyar, R.S., Scott, J.F., Kohlstedt, H., Petraru, A., Hwang, C.S.: Emerging memories: resistive switching mechanisms and current status. Rep. Prog. Phys **75**, 076502 (2012)
27. Yang, J.J., Pickett, M.D., Li, X., Ohlberg, D.A.A., Stewart, D.R., Williams, R.S.: Memristive switching mechanism for metal/oxide/metal nanodevices. Nat. Nanotechnol. **3**, 429 (2008)
28. Yang, J.J., Borghetti, J., Murphy, D., Stewart, D.R., Williams, R.S.: A family of electronically reconfigurable nanodevices. Adv. Mater. **21**, 3754 (2009)
29. Waser, R., Dittmann, R., Staikov, G., Szot, K.: Redox-based resistive switching memories–nanoionic mechanisms, prospects, and challenges. Adv. Mater. **21**, 2632 (2009)
30. Chua, L.: If it's pinched it'sa memristor. Semicond. Sci. Technol. **29**, 104001 (2014)
31. Valov, I., Linn, E., Tappertzhofen, S., Schmelzer, S., Hurk, J.V.D., Lentz, F., Waser, R.: Nanobatteries in redox-based resistive switches require extension of memristor theory. Nat. Commun. **4**, 1771 (2013)
32. Qingjiang, L., Khiat, A., Salaoru, I., Papavassiliou, C., Hui, X., Prodromakis, T.: Memory impedance in TiO_2 based metal-insulator-metal devices. Sci. Rep. **4**, 4522 (2014)
33. Jo, S.H., Chang, T., Ebong, I., Bhadviya, B.B., Mazumder, P., Lu, W.: Nanoscale memristor device as synapse in neuromorphic systems. Nano Lett. **10**, 1297 (2010)
34. Dongale, T.D., Desai, N.D., Khot, K.V., Mullani, N.B., Pawar, P.S., Tikke, R.S., Patil, V.B., Waifalkar, P.P., Patil, P.B., Kamat, R.K., Patil, P.S., Bhosale, P.N.: Effect of surfactants on the data directionality and learning behaviour of Al/TiO_2/FTO thin film

memristor-based electronic synapse. J. Solid State Electron. **21**, 2753 (2017)
35. Dongale, T.D., Pawar, P.S., Tikke, R.S., Mullani, N.B., Patil, V.B., Teli, A.M., Khot, K.V., Mohite, S.V., Bagade, A.A., Kumbhar, V.S., Rajpure, K.Y., Bhosale, P.N., Kamat, R.K., Patil, P.S.: Mimicking the synaptic weights and human forgetting curve using hydrothermally grown nanostructured CuO memristor device. J. Nanosci. Nanotechnol. **18**, 984 (2018)
36. Dongale, T.D., Khot, K.V., Mali, S.S., Patil, P.S., Gaikwad, P.K., Kamat, R.K., Bhosale, P.N.: Development of Ag/ZnO/FTO thin film memristor using aqueous chemical route. Mater. Sci. Semicond. Process. **40**, 523 (2015)
37. Dongale, T.D., Mohite, S.V., Bagade, A.A., Gaikwad, P.K., Patil, P.S., Kamat, R.K., Rajpure, K.Y.: Development of Ag/WO_3/ITO thin film memristor using spray pyrolysis method. Electron. Mater. Lett. **11**, 944 (2015)
38. Dongale, T.D., Shinde, S.S., Kamat, R.K., Rajpure, K.Y.: Nanostructured TiO_2 thin film memristor using hydrothermal process. J. Alloys Compd. **593**, 267 (2014)
39. Ventra, M.D., Pershin, Y.V.: On the physical properties of memristive, memcapacitive and meminductive systems. Nanotechnology **24**, 255201 (2013)
40. Han, J., Song, C., Gao, S., Wang, Y., Chen, C., Pan, F.: Realization of the meminductor. ACS Nano **8**, 10043 (2014)
41. Saraf, S., Markovich, M., Vincent, T., Rechter, R., Rothschild, A.: Memory diodes with nonzero crossing. Appl. Phys. Lett. **102**, 022902 (2013)
42. Tappertzhofen, S., Linn, E., Bottger, U., Waser, R., Valov, I.: Nanobattery effect in RRAMs-implications on device stability and endurance. IEEE Electron Device Lett. **35**, 208 (2014)
43. Biolek, D., Biolek, Z., Biolkova, V.: Pinched hysteretic loops of ideal memristors, memcapacitors and meminductors must be 'self-crossing'. Electron. Lett. **47**, 1385 (2011)
44. Pershin, Y.V., Di Ventra, M.: Memory effects in complex materials and nanoscale systems. Adv. Phys. **60**, 145 (2011)
45. You, Y.H., So, B.S., Hwang, J.H., Cho, W., Lee, S.S., Chung, T.M., Kim, C.G., An, K.S.: Impedance spectroscopy characterization of resistance switching NiO thin films prepared through atomic layer deposition. Appl. Phys. Lett. **89**, 222105 (2006)
46. Greenlee, J.D., Calley, W.L., Moseley, M.W., Doolittle, W.A.: Comparison of interfacial and bulk ionic motion in analog memristors. IEEE Trans. Electron Devices **60**, 427 (2013)